

END-TO-END 9-D POLARIZED BUNCH TRANSPORT IN eRHIC ENERGY-RECOVERY RECIRCULATOR, SOME ASPECTS

F. Méot, S. Brooks, V. Ptitsyn, D. Trbojevic, N. Tsoupas
 Collider-Accelerator Department, BNL, Upton, NY 11973, USA

Abstract

This paper is a brief overview of some of the numerous beam and spin dynamics investigations undertaken in the framework of the design of the FFAG based electron energy recovery re-circulator ring of the eRHIC electron-ion collider project.

INTRODUCTION

A Fixed Field Alternating Gradient (FFAG) doublet-cell version of the energy recovery recirculator of the eRHIC electron-ion collider is being investigated [1]. A pair of such FFAG rings placed along RHIC recirculate the electron beam through a 1.322 GeV linac (ERL), from respectively 1.3 to 6.6 GeV (5 beams) and 7.9 to 21.2 GeV (11 beams), and back down to injection energy. A spreader and a combiner are placed at the linac ends for proper orbit and 6-D matching, including time-of-flight adjustment.

FFAG LATTICE

The second, 11 beam, 21.2 GeV ring is considered in this discussion since it produces the major SR induced particle and spin dynamics perturbations. The cell is shown in Fig. 1, there are 138 such cells in each one of the 6 eRHIC arcs. The 6 long straight sections (LSS) use that very cell, with quadrupole axes aligned. In the twelve, 17-cell, dispersion suppressors (DS) the quadrupole axes slowly shift from their distance in the arc, to zero at the LSS.

Fig. 2 shows the transverse excursion and magnetic field along orbits across the arc cell. Fig. 3 shows the energy dependence of the deviation angle and curvature radius in the two quadrupoles, and the energy dependent tunes and chromaticities.

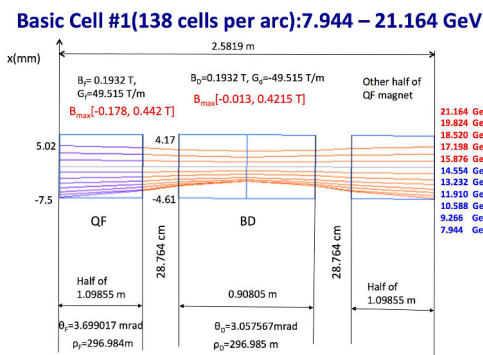


Figure 1: Arc cell in the 7.944-21.16 GeV recirculating ring.

The y -precession of the spin over the six 138-cell arcs amounts to $6 \times 138 \times a\gamma\theta_{\text{cell}} = a\gamma \times (2\pi - 0.688734)$ rad

(with the difference to $a\gamma \times 2\pi$ corresponding to the contribution of the 12 DS), *i.e.*, from 18 precessions at 7.944 GeV to 48 at 21.164 GeV. ($a = 0.00116$ is the electron anomalous magnetic factor, γ the Lorentz relativistic factor).

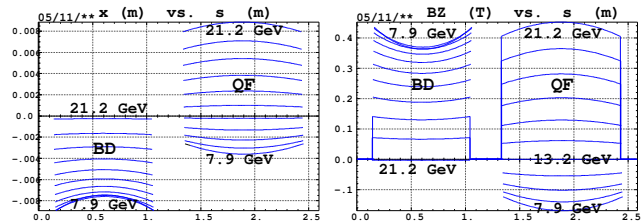


Figure 2: Transverse excursion in the quadrupole frame (hence artefact of trajectory discontinuity) (left) and hard-edged magnetic field (right), along the 11 orbits across the arc FFAG cell.

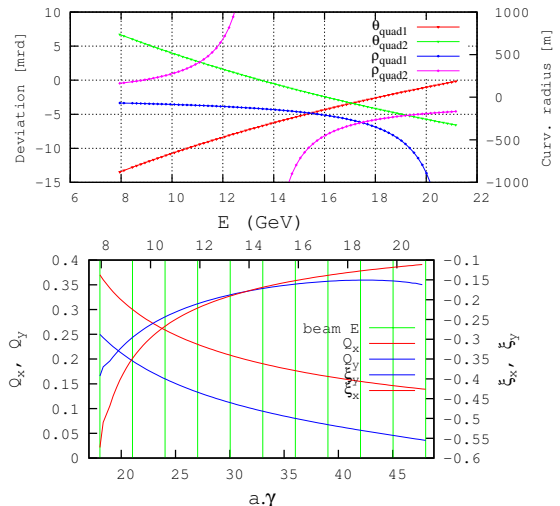


Figure 3: Top : energy dependence of deviation and curvature radius in arc cell quads. Bottom : cell tunes and chromaticities; the vertical bars materialize the 11 design energies.

SYNCHROTRON RADIATION

The SR induced energy loss relative to the the bunch centroid and the energy spread write, respectively

$$\frac{\overline{\Delta E}}{E_{\text{ref}}} = 1.9 \times 10^{-15} \frac{\gamma^3 \Delta\theta}{\rho}, \quad \frac{\sigma_E}{E_{\text{ref}}} = 3.8 \times 10^{-14} \frac{\gamma^{5/2} \sqrt{\Delta\theta}}{\rho} \quad (1)$$

with $\Delta\theta$ the arc length and $1/\rho$ the curvature, assumed constant. Taking for average radius, in the QF (focusing quad) and BD (defocusing quad) magnets respectively, $\rho_{\text{BD}} \approx \frac{s_{\text{BD}}}{\Delta\theta_{\text{BD}}}$, $\rho_{\text{QF}} \approx \frac{s_{\text{QF}}}{\Delta\theta_{\text{QF}}}$ (with s_{BD} and s_{QF} the arc lengths) and considering in addition, with l_{BD} , l_{QF} the magnet lengths, $s_{\text{BD}} \approx l_{\text{BD}}$, $s_{\text{QF}} \approx l_{\text{QF}}$, then one gets,

per cell

$$\overline{\Delta E} [MeV] \approx 0.96 \times 10^{-15} \gamma^4 \left(\frac{l_{BD}}{\rho_{BD}^3} + \frac{l_{QF}}{\rho_{QF}^3} \right) \quad (2)$$

Taking in addition $\langle (1/\rho)^2 \rangle \approx 1/\langle \rho^2 \rangle$, an estimate of the energy spread is

$$\sigma_E \approx 1.94 \times 10^{-14} \gamma^{7/2} \sqrt{\frac{l_{BD}}{|\rho_{BD}^3|} + \frac{l_{QF}}{|\rho_{QF}^3|}} \quad (3)$$

This is illustrated for a complete eRHIC turn (including LSS and DS sections) in Fig. 4, where it is also compared with Monte Carlo tracking, the agreement is at % level. The energy loss shows a local minimum in the $a\gamma = 30-35$ region, a different behavior from the classical γ^4 dependence in an isomagnetic lattice.

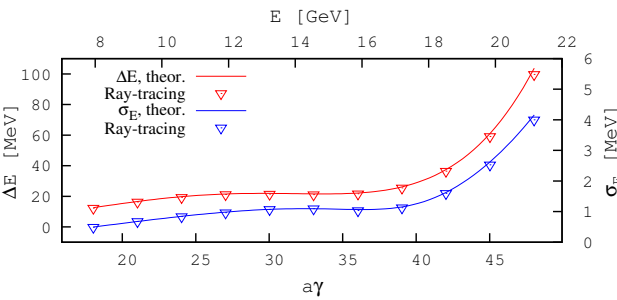


Figure 4: Energy loss and energy spread. Solid lines : theory (Eqs. 2 and 3) for a 6-arc ring. Markers : Monte Carlo, for a complete eRHIC ring (see sample tracking outcomes in Fig. 5).

The bunch lengthening over a $[s, s_f]$ distance, resulting from the stochastic energy loss, can be written [2],

$$\sigma_l = \left(\frac{\sigma_E}{E} \right) \left[\frac{1}{L_{bend}} \int_s^{s_f} (D_x(s)T_{51}(s_f \leftarrow s) + D'_x(s)T_{52}(s_f \leftarrow s) - T_{56})^2 ds \right]^{1/2} \quad (4)$$

with the integral being taken over the bends, D_x and D'_x the dispersion function and its derivative, T_{5i} the trajectory lengthening coefficient of the first order mapping ($i = 1, 5, 6$ stand for respectively $x, \delta l, \delta p/p$ coordinates).

The energy loss causes a drift of the bunch centroid, as well as an horizontal emittance increase, both can be computed from the lattice parameters in the linear approximation [2, 3, 4]. Fig. 6 illustrates these effects over a 21.164 GeV recirculation (with bunch re-centering on the reference optical axis at each of the six LSS).

Cumulative effect of SR, over a complete 7.94→21.2→7.94 GeV cycle, is illustrated in Fig. 7 : (i) energy spread, $\sigma_E/E = 2.6 \times 10^{-4}$ at 21.1 GeV and $\sigma_E/E = 8.4 \times 10^{-4}$ back at 7.944 GeV ; (ii) bunch lengthening, $\sigma_l = 2$ mm at 21.1 GeV and $\sigma_l = 2.5$ mm back down to 7.944 GeV ; (iii) normalized horizontal emittance (from zero starting value), namely, $\epsilon_x = 20 \mu\text{m}$ at 21.1 GeV (with strong contribution from uncompensated chromatic effects), and $\epsilon_x = 8 \mu\text{m}$ back at 7.944 GeV.

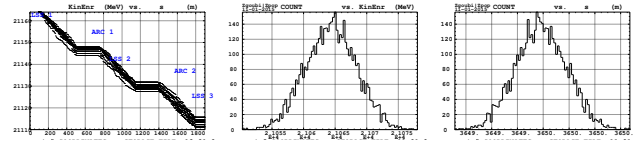


Figure 5: Left : stochastic energy decrease of a few particles over the first 3 arcs at $E_{ref} = 21.164$ GeV. Middle : final energy spread a 5000 particle bunch after the 21.164 GeV pass, $\frac{\sigma_E}{E_{ref}} = 1.9 \times 10^{-4}$ around $\frac{\Delta E}{E_{ref}} = -4.7 \times 10^{-3}$ average energy loss (Eq. 1). Right : longitudinal bunch distribution (Eq. 4).

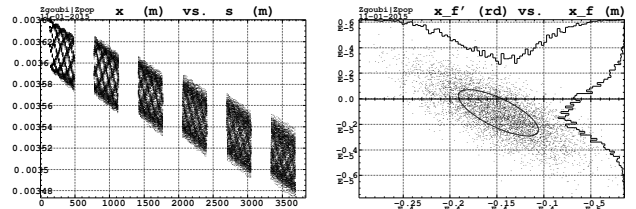


Figure 6: Left : SR loss induced x-drift along the 6 arcs, complete ring, $E = 21.164$ GeV, (shown are a few particles in a bunch launched on the LSS axis with zero initial 6-D emittance). Right : a 5000 particle bunch, horizontal phase space after that complete turn, featuring $\overline{x_f} = -15 \mu\text{m}$, $\sigma_{x_f} = 4.3 \mu\text{m}$, $\overline{x'_f} = -1.1 \mu\text{rad}$, $\sigma_{x'_f} = 1.8 \mu\text{rad}$.

Chromaticity

The natural chromaticity combined with energy spread cause a betatron phase extent of the bunch and thus emittance growth. Off-centering of the bunch causes even greater apparent emittance increase. This effect of the chromaticity constrains the tolerances on magnet alignment and field defects [5].

Acceptance

The naturally large dynamical acceptance of the linear lattice shrinks with magnet alignment and field defects, this is illustrated in Fig. 8. SR is off in these DA computations, SR causes emittance growth thus reducing the space available for the beam at injection into a recirculation.

Multipole Defects

Fig. 9 illustrates a different way of looking at tolerances, e.g. here in the presence of a dodecapole defect in all quadrupoles of the ring (i.e., same working hypotheses as for the bottom Fig. 8) : a 5000-particle bunch is launched with $\epsilon_x \approx \epsilon_y \approx 50 \mu\text{m}$ and 10^{-4} rms energy spread, for 21 circulations in a complete ring ($6 \times [\frac{1}{2}\text{LSS} - \text{DS} - \text{ARC} - \text{DS} - \frac{1}{2}\text{LSS}] + \text{Linac}$). SR loss is summarily compensated at the linac, bunch position is assumed perfectly corrected at each LSS. Fig. 9 shows the emittance evolution, pass after pass, from 7.94 to 21.16 and back to 7.94 GeV. This gives an indication of the maximum tolerable defect, depending on criteria of maximum tolerable emittance, e.g. at collision (pass 11) and/or extraction (pass 21).

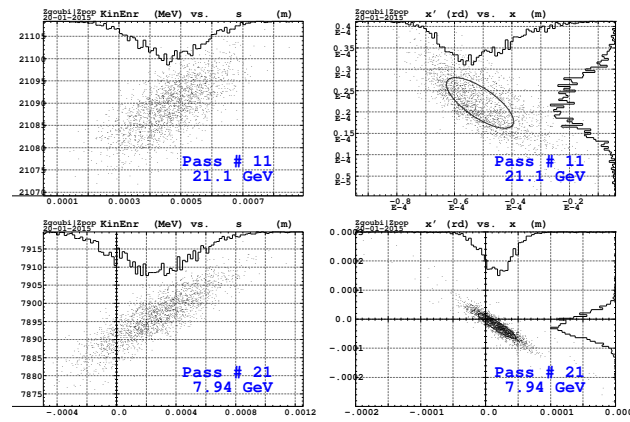


Figure 7: Cumulated effects of SR, in longitudinal (left) and radial (right) phase space, over 21 passes in eRHIC (from 7.944 GeV to 21.164 GeV, and back down to 7.944 GeV). Left plots : energy spread and bunch lengthening. Right plots : horizontal emittance growth.

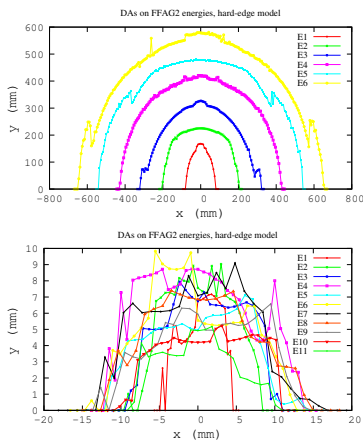


Figure 8: Available injection window into the ring at mid-LSS, for each of the 11 beams, observed at the center of an LSS. Top : defect-free lattice. Bottom : in the presence of dodecapole defect, ± 3 Gauss at 1 cm, random uniform.

POLARIZATION

Polarized electron bunch production is based on a Gatling gun, with a polarization of 85-90%. The electron bunch is re-circulated in eRHIC with longitudinal polarization. Spins precess at a rate $a\gamma$ per turn, with an increment of $a\Delta\gamma = 3$ at each 1.322 GeV linac boost, so ensuring the requested longitudinal spin orientation at the two IPs.

Depolarization mainly stems from energy spread (e.g., a cumulated $2.5 \cdot 10^{-4}$ at 21.2 GeV from SR contribution, see Fig. 7). Spin diffusion resulting from stochastic SR also causes polarization loss, of about 2% at 21.2 GeV. Non-zero vertical emittance, or vertical defects, cause spins to leave the median plane. This is illustrated in Fig. 10.

Fig. 11 monitors the evolution of the polarization and of spin angle spreading, in the conditions of dodecapole error simulations discussed earlier (“Multipole defect” section and Fig. 9). Both quantities appear unchanged in this particular case, compared to the unperturbed optics (cf. σ_ϕ

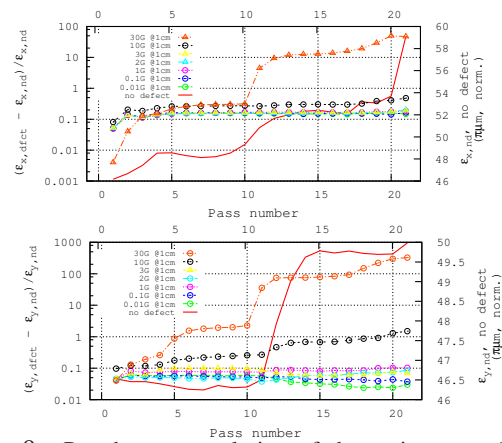


Figure 9: Pass-by-pass evolution of the emittances of a re-circulated bunch, for various dodecapole defect strengths (from 0, to 10 Gauss at 1 cm). Left axis and markers : defect cases. Right axis and red curve : defect-free ring. Top : horizontal, bottom : vertical emittances.

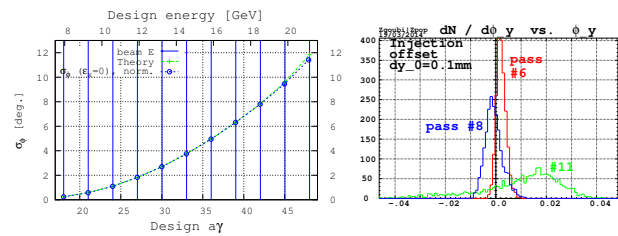


Figure 10: Polarization loss. Left : from energy spread, including theoretical expectation [6]. Right : vertical spin angle spread, in the presence of initial vertical beam jitter.

in Fig. 10-left).

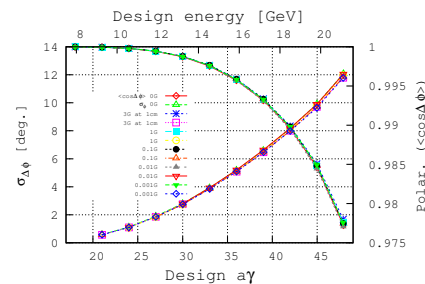


Figure 11: Polarization (right vertical axis) and spin angle spread (left axis) in the presence of dodecapole errors.

REFERENCES

- [1] E.C. Aschenauer et al., “eRHIC Design Study, Electron-Ion Collider at BNL”, arXiv:1409.1633, Sept. 2014.
- [2] G. Leleux et al., Synchrotron radiation perturbation in transport lines, Part. Acc. Conf., San Francisco, May 6-9, 1991.
- [3] https://oraweb.cern.ch/pls/hhh/code_website?code_name=BETA
- [4] F. Méot, J. Payet, Simulation of SR loss in high energy transport lines, Rep. CEA DSM DAPNIA/SEA-00-01 (2000).
- [5] F. Méot, C. Liu, Chromatic Effects and Orbit Correction in eRHIC FFAG Arcs, IPAC15, these proceedings (TUPWI055).
- [6] V. Ptitsyn, Electron Polarization Dynamics in eRHIC, EIC 14 workshop, JLab, 17-21/03/2014.